Thermal Denaturation of Ribonuclease A Characterized by Water ^{17}O and ^{2}H Magnetic Relaxation Dispersion[†]

Vladimir P. Denisov and Bertil Halle*

Condensed Matter Magnetic Resonance Group, Department of Chemistry, Lund University, P.O. Box 124, S-22100 Lund, Sweden

Received February 24, 1998; Revised Manuscript Received April 14, 1998

ABSTRACT: Water oxygen-17 and deuteron nuclear magnetic relaxation dispersion (NMRD) measurements were used to characterize ribonuclease A (RNase A) in the course of thermal denaturation at pH* 2 and 4. The structure and dynamics of the protein were probed by specific long-lived water molecules, by the short-lived surface hydration, and by labile side-chain hydrogens. The NMRD data show that native RNase A contains at least three water molecules with a mean residence time of 8 ns at 27 °C and an activation enthalpy of ca. 40 kJ mol^{-1}. These water molecules are identified with some or all of six ordered water molecules partly buried in surface pockets in the crystal structure of RNase A. The loss of the ^{17}O dispersion at higher temperatures demonstrates that, in the thermally denatured protein, these surface pockets are either not present or undergoing large structural fluctuations on a subnanosecond time scale. The relaxation dispersion step vanishes monotonically and essentially in concert with the CD denaturation curves, thus ruling out the existence of equilibrium intermediates with a substantial amount of non-native and long-lived hydration water. The NMRD data show that thermally denatured RNase A has a relatively compact but highly flexible structure. The global solvent exposure and the hydrodynamic volume of the denatured protein are much less than for maximally unfolded disulfide-intact RNase A. The NMRD data show that thermal denaturation is accompanied by a large reduction of the mean-square orientational order parameter of side-chain O−H bonds, implying that, in the denatured state, these side chains sample a wide distribution of conformational states on a subnanosecond time scale.

The denatured states of globular proteins range from random coils to compact structures with nativelike secondary structure (*1*−*4*). Although physiologically inactive, the partially folded states formed under non-native conditions of temperature, pH, or solvent composition can provide important insights about the determinants of protein stability (*5, 6*) and the mechanism of protein folding (*7*−*9*).

Being less ordered than the native protein, denatured states are inherently less amenable to high-resolution structural analysis. A variety of experimental methods have been used to illuminate different aspects of denatured proteins, frequently with conflicting results. One particularly controversial aspect concerns hydration changes on denaturation, directly related to the hydrophobic effect that is widely held to be a major driving force for protein folding (*2, 6, 10, 11*). The available experimental information about hydration of denatured proteins is largely derived in an indirect way from macroscopic properties, such as calorimetric data (*12*) or density and sound velocity (*13*). Computer simulations can in principle provide a detailed picture of hydration (*14*−*17*), but it is not clear to what extent the artificially perturbed states studied by computer simulation resemble real proteins denatured under equilibrium conditions (*18*). A more detailed experimental characterization of hydration changes on protein denaturation would therefore seem to be needed.

In the present work, we use the nuclear magnetic relaxation dispersion (NMRD) of the water ^{17}O and ^{2}H nuclei to study the thermal denaturation of RNase A[1] in aqueous solution at acidic pH. The $^{17}O/^{2}H$ NMRD method has previously been used mainly to characterize the order and dynamics of specific long-lived water molecules in proteins (*19, 20*) and oligonucleotides (*21*). As demonstrated here, the NMRD method can also monitor changes in structure and hydration in the course of protein denaturation. Long-lived water molecules residing in cavities or surface pockets can be exploited as intrinsic probes of the structural integrity of the protein, while the amount of dynamically retarded water in contact with the protein surface is an indicator of global solvent exposure. In addition, NMRD data provide information about the flexibility (orientational order parameter) of side chains containing labile hydrogens and about the compactness (hydrodynamic volume) of the protein.

Bovine pancreatic ribonuclease A has been extensively studied by a variety of biochemical and biophysical methods. It consists of three helices and a large β-sheet region, and

[†] This work was supported by the Swedish Natural Science Research Council and the Royal Swedish Academy of Sciences.

* Author to whom correspondence should be addressed.

[1] Abbreviations: BPTI, bovine pancreatic trypsin inhibitor; CD, circular dichroism; DLS, dynamic light scattering; FTIR, Fourier transform infrared; GdmCl, guanidinium chloride; NMRD, nuclear magnetic relaxation dispersion; RNase A, bovine pancreatic ribonuclease A.

S0006-2960(98)00442-5 CCC: $15.00
Published on Web 06/12/1998

the main-chain fold in solution (*22*) is virtually the same as in the crystal (*23*). RNase A is among the few proteins that do not contain buried water molecules, but the crystal structure identifies several water molecules in surface pockets (*23*). Some of these semiburied water molecules are likely to have residence times in the nanosecond to microsecond range and, hence, are thought to be responsible for the previously reported ^{17}O relaxation dispersion from an RNase A solution (*19*).

As is the case for many proteins (*1*), the thermally denatured form of RNase A is more compact than the GdmCl denatured form, and the native as well as the denatured states are further unfolded on reduction of the four disulfide bonds (*24, 25*). The thermal denaturation of RNase A is reversible and appears to be a two-state transition, at least at low pH (*26*−*28*).

Whereas several CD, NMR, and FTIR studies have suggested that the thermally denatured state of RNase A retains some degree of secondary structure (*29*−*32*), two recent FTIR studies suggested that all native secondary structure is disrupted by thermal denaturation (*33, 34*). Each of these opposing views is supported by results from other techniques. A quenched-flow NMR study showed no significant hydrogen-exchange protection at pH* 1.5−3.8 and 65 °C, suggesting that thermally denatured RNase A contains no stable secondary structure (*35*).

Calorimetric studies, showing that the heat capacity of thermally denatured proteins is essentially the same as that of the constituent amino acid side chains, have been taken to imply that thermally denatured RNase A is extensively unfolded and that the nonpolar side chains forming the native hydrophobic core are fully hydrated (*36, 37*). Changes in the apparent molar volume and adiabatic compressibility on thermal denaturation of RNase A have also been attributed to extensive exposure of nonpolar side chains (*13*).

In the following, we report the water ^{17}O and ^{2}H relaxation dispersion profiles from aqueous RNase A solutions at pH* 2 and 4 at seven temperatures in the range 4−65 °C where the thermal transition occurs. These data show that thermally denatured RNase A is relatively compact, but flexible. The hydrodynamic volume and solvent exposure are much smaller than expected for a fully unfolded conformation, but the complete loss of long-lived water sites at the protein surface and the large reduction of side-chain orientational order indicate substantial conformational flexibility in the denatured state.

MATERIALS AND METHODS

Sample Preparation. Bovine pancreatic ribonuclease A (type XII-A) was purchased from Sigma and further purified by chromatography on CM-Sephadex, eluting with a linear salt gradient (0−0.3 M NaCl in 10 mM Tris-HCl buffer, pH 8.0). The dominant fraction was dialyzed against pure water and then lyophilized. Protein solutions were made from ^{17}O-enriched D_2O (21.9 at. % ^{17}O, 61.9 at. % ^{18}O, 99.95 at. % ^{2}H) obtained from Ventron (Karlsruhe). pH* (the direct reading from a D_2O solution after calibration with standard H_2O buffers) was measured with a Radiometer PHM63 digital pH meter equipped with a 5-mm combination electrode. The protein was studied at pH* 2.0 and 4.0, adjusted (at room temperature) by minute additions of concentrated HCl or NaOH.

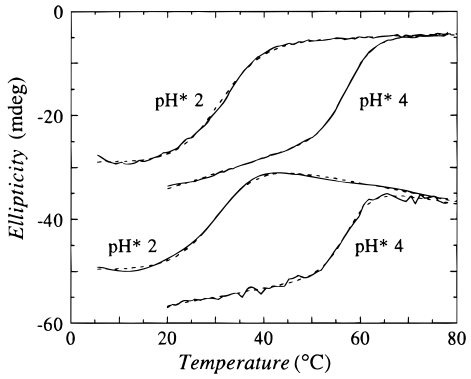

FIGURE 1: Temperature dependence of the ellipticity of RNase A solutions at pH* 2.0 and 4.0. The ellipticity was recorded at 275 nm (upper pair of curves) and 222 nm (lower pair of curves) on the samples used for NMRD measurements after dilution to an RNase A concentration of 1.25 mM (275 nm) or 63 μM (222 nm). The solid and dashed curves refer to experimental data and fits, respectively.

The protein concentration in the NMR samples was determined from the optical absorption at 280 nm (after 30-fold dilution in 6 M GdmCl and 20 mM phosphate, pH 6.5), using the calculated (*38*) extinction coefficient $\epsilon_{280} = 8.64$ mM^{-1} cm^{-1}. The RNase A concentration, 3.76 ± 0.10 mM, determined in this way corresponds to 14 140 ± 400 water molecules per protein molecule.

Circular Dichroism Measurements. Near-UV (275 nm) and far-UV (222 nm) CD measurements were performed on a JASCO J-720 spectropolarimeter equipped with a PTC-343 Peltier-type thermostatic cell holder, which was calibrated with a copper−constantan thermocouple. For the CD measurements, the NMRD samples were diluted with D_2O and adjusted to pH* 2.0 or 4.0. Temperature scans were performed with a step resolution of ca. 1 °C and a scan rate of 20 °C h^{-1}. Both samples exhibited CD profiles characteristic of thermal denaturation (*31, 35*), with the same denaturation temperature, T_d, at 222 and 275 nm (see Figure 1). CD profiles obtained on heating and cooling were identical within experimental accuracy (ca. 2%), demonstrating that the denaturation transition is fully reversible under our conditions.

The CD data were analyzed with the usual two-state model with linearly temperature-dependent ellipticity in the native and denatured states. The fraction, f_N, native protein was parametrized as

$$f_N(T) = [1 + 9^{2T_d(1-T_d/T)/\Delta T}]^{-1} \quad (1)$$

with the transition width, ΔT, defined as the temperature difference between the points of 10 and 90% native population. This relation follows from the two-state model, assuming a temperature-independent heat capacity difference and a reasonably narrow transition ($\Delta T \ll T_d$). Fits to the combined near- and far-UV CD data (dashed curves in Figure 1) yielded $T_d = 30.9$ °C and $\Delta T = 19.2$ °C at pH* 2.0 and $T_d = 57.6$ °C and $\Delta T = 11.8$ °C at pH* 4.0, with an estimated uncertainty of ±0.4 °C in T_d. These denaturation temperatures agree well with literature data (*26, 31, 39*).

Magnetic Relaxation Measurements. The longitudinal relaxation rate, R_1, of the ^{17}O and ^{2}H nuclei in water was measured at seven temperatures in the range 4−65 °C and at 10 magnetic fields in the range 0.38−14.1 T, using one

Table 1: Parameters Derived from ^{17}O NMRD Data

T (°C)	pH*	$10^{-3}\alpha N_T/R_{bulk}$	$\beta N_T/\omega_Q^2$	τ_β (ns)	R_{bulk} (s^{-1})
4	2	2.7 ± 0.2	2.2 ± 0.3	10.9 ± 1.4	370
	4	3.1 ± 0.2	2.5 ± 0.2	11.8 ± 1.0	
15	2	2.3 ± 0.1	2.0 ± 0.2	6.0 ± 0.4	251.3
	4	2.7 ± 0.1	2.0 ± 0.2	7.7 ± 0.7	
27	2	1.8 ± 0.1	2.2 ± 0.3	2.9 ± 0.2	175
	4	2.1 ± 0.1	2.3 ± 0.2	3.6 ± 0.3	
35	2	1.8 ± 0.1	1.1 ± 0.3	3.1 ± 0.5	142.5
	4	1.9 ± 0.2	2.1 ± 0.3	2.9 ± 0.3	
45	2	1.7± 0.1	0.5 ± 0.1	2.0[a]	113.8
	4	1.8± 0.4	1.7 ± 0.9	1.9 ± 0.5	
55	2	1.60 ± 0.03	0[a]		93.2
	4	1.5[a]	1.3 ± 0.3	1.3 ± 0.3	
65	2	1.32 ± 0.07	0[a]		77.8
	4	1.51 ± 0.06	0[a]		

[a] Parameter value frozen in the fit.

Table 2: Parameters Derived from ^2H NMRD Data [a]

T (°C)	pH*	$10^{-3}\alpha N_T/R_{bulk}$	$\beta_L(10^8\ s^{-2})$	τ_R (ns)	R_{bulk} (s^{-1})
4	2	2.6 ± 0.1	2.1 ± 0.1	14.2 ± 0.7	4.74
	4	2.7 ± 0.2	0.9 ± 0.1	17.1 ± 2.3	
15	2	1.9 ± 0.2	2.9 ± 0.2	8.0 ± 0.4	3.25
	4	2.3 ± 0.2	1.3 ± 0.1	10.4 ± 1.0	
27	2	2.0 ± 0.3	2.6 ± 0.2	6.6 ± 0.6	2.26
	4	2.0 ± 0.1	1.6 ± 0.1	6.9 ± 0.4	
35	2	2.2 ± 0.2	2.0 ± 0.2	6.1 ± 0.5	1.85
	4	2.0 ± 0.2	1.5 ± 0.1	6.2 ± 0.5	
45	2	2.4± 0.2	1.1 ± 0.1	5.2 ± 0.5	1.48
	4	2.0± 0.3	1.7 ± 0.2	4.6 ± 0.6	
55	2	2.4 ± 0.2	0.7 ± 0.1	4.2 ± 0.5	1.21
	4	2.1 ± 0.5	1.5 ± 0.3	3.8 ± 0.7	
65	2	2.3 ± 0.2	0.6 ± 0.1	3.0 ± 0.5	1.01
	4	2.5 ± 0.3	0.7 ± 0.2	3.3 ± 0.7	

[a] From bi-Lorentzian fits with water parameters from ^{17}O data and $S^2(^2H)/S^2(^{17}O) = 0.366$.

field-variable (iron magnet) and four fixed-field (cryomagnet) NMR spectrometers (*20, 40*). All NMRD measurements were carried out on two samples, one at pH* 2.0 and the other at pH* 4.0. Since both magnetic field and temperature were varied in a nonmonotonic way, the smooth variation of the NMRD parameters (vide infra) can be taken as evidence that irreversible aggregation and/or denaturation did not occur to a significant extent. This was also indicated by the reversibility of the CD profiles and the finding that the NMRD samples remained completely homogeneous and transparent even half a year after preparation. The relaxation rate, R_{bulk}, of a bulk water sample with the same isotope composition as the solvent in the protein solutions was measured at 4, 15, 27, 42, 60, and 80 °C, and the values at intermediate temperatures were obtained by interpolation (see Tables 1 and 2).

Analysis of ^{17}O NMRD Data. Water ^{17}O NMRD profiles from protein solutions are usually described accurately by the theoretical expression (*20, 41*)

$$R_1 = R_{bulk} + \alpha + \beta[0.2j(\omega_0) + 0.8j(2\omega_0)] \qquad (2)$$

with a Lorentzian spectral density function $j(\omega) = \tau_\beta/[1 + (\omega\tau_\beta)^2]$. Here, ω_0 is the variable resonance frequency and τ_β is the correlation time.

The ^{17}O NMRD profiles from solutions of RNase A at pH* 2.0 and 4.0 and at seven temperatures spanning the range of thermal denaturation are shown in Figure 2. To facilitate

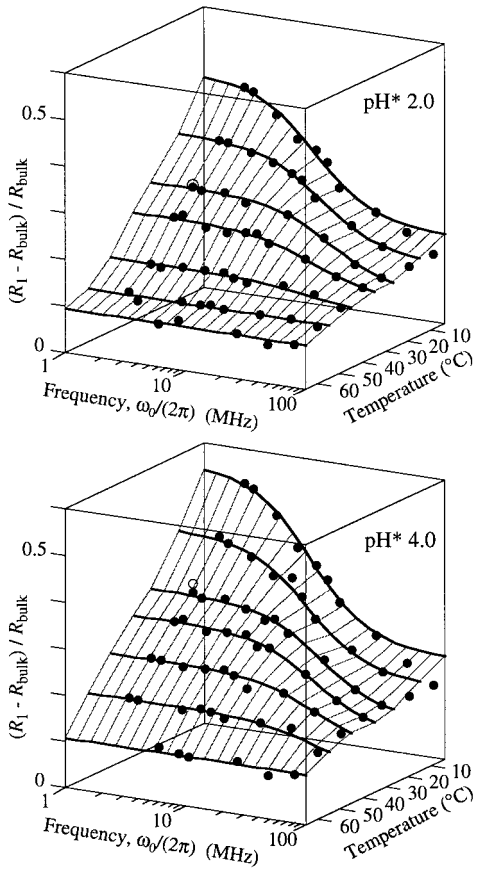

FIGURE 2: Frequency dependence of water ^{17}O longitudinal relaxation rate, R_1, normalized with the bulk water relaxation rate, from 3.76 mM solutions of RNase A in D_2O at pH* 2.0 (top) and pH* 4.0 (bottom) and at seven temperatures. The fitted curves are described by eq 2, with parameters according to Table 1. The transverse relaxation rate was measured at 27 °C and at the lowest frequency (open circles).

comparison of NMRD profiles at different temperatures, the excess relaxation rate, $R_1 - R_{bulk}$, normalized with R_{bulk} is plotted. The curves are fits of the theoretical dispersion function in eq 2, and the resulting values of the parameters α, β, and τ_β are given in Table 1. The data conform well to the expected Lorentzian dispersion shape, except at the lowest temperatures (4 and 15 °C). Here, the two highest frequency points (48 and 81 MHz) fall below the high-frequency plateau of the Lorentzian dispersion, suggesting a second dispersion step from water molecules with residence times of ca. 1 ns (cf. the 55 °C dispersion at pH* 4, with $\tau_\beta = 1.3$ ns). For consistency in the analysis of the temperature dependence of the α and β parameters, the fits were done without the 48 and 81 MHz points at 4 °C and the 81 MHz point at 15 °C. The relaxation contribution from the water molecules responsible for the high-frequency dispersion is thus included in the α term at all temperatures. At 65 °C (and at 55 °C for pH* 4), no significant dispersion was detected in the investigated frequency range; only the α parameter was then determined from the data. In two cases, where only the low-frequency part of the dispersion was accessible, one of the three parameters was frozen in the fit (see Table 1).

The transverse relaxation rate, R_2, was measured at 27 and 35 °C at the lowest field (27 °C data shown as open circles in Figure 2). The finding (at both temperatures) that R_2 equals R_1 within experimental error demonstrates that the

low-frequency plateau of the dispersion has been reached, i.e., there can be no further dispersion step at lower frequencies (*20*). A low-frequency dispersion step would be produced by protein aggregates with long tumbling times. The observed equality of R_2 and R_1 at low field thus shows that protein aggregation is unimportant under our conditions (3.8 mM RNase A). This is in line with the finding that the thermal denaturation curves recorded by ^{1}H NMR spectroscopy are superimposable at concentrations of 0.5 and 5 mM RNase A (*35*). While protein aggregates thus appear not to be present, some protein−protein interaction (at least at pH* 4.0) is indicated by the pH dependence of the rotational correlation time (vide infra). Such interactions may complicate the interpretation of the rotational correlation time in terms of a hydrodynamic volume. As long as the interactions do not perturb the structure of the hydrated protein, however, they should have little effect on the amplitude parameters α and β or on the derived water residence time.

The physical significance of the parameters of eq 2 has been established in previous studies of aqueous solutions of a range of (native) proteins (*19, 20*). It is convenient to scale the parameters α and β according to (*20*)

$$\alpha N_T/R_{bulk} = N_\alpha \rho \tag{3}$$

$$\beta N_T/\omega_Q{}^2 = N_\beta S^2 \tag{4}$$

N_T is the overall water/protein mole ratio and can be calculated from the composition of the sample (vide supra). N_α is the number of short-lived water molecules in contact with the protein surface, and $\rho = (\tau_\alpha/\tau_{bulk} - 1)$ is their average dynamic retardation factor. N_β is the number of long-lived water molecules associated with the protein, with residence time $\tau_W > 1$ ns and root-mean-square orientational order parameter S. The asymmetry parameter of the electric field gradient tensor was previously (*19*) included in the order parameter (then denoted A_I), but is now incorporated in the rigid-lattice quadrupole frequency, $\omega_Q = 7.61 \times 10^6$ rad s^{-1} for ^{17}O and 8.70×10^5 rad s^{-1} for ^{2}H (*20*). With the present convention, a water molecule that tumbles rigidly with the protein has $S = 1$ for both nuclei.

The correlation time τ_β defines the time scale for orientational randomization of long-lived water molecules by rotational diffusion of the protein, with correlation time τ_R, and/or by exchange of such water molecules with bulk water at a rate $1/\tau_W$. Since these processes are independent, their rates are additive and (*20*)

$$1/\tau_\beta = 1/\tau_R + 1/\tau_W \tag{5}$$

In the transition region, where the native and denatured states are both significantly populated, the observed (exchange-averaged) relaxation rate is a population-weighted average:

$$R_1 = f_N R_{1N} + (1 - f_N) R_{1D} \tag{6}$$

In principle, the NMRD profile should then be described by a bi-Lorentzian dispersion function, with different correlation times for the native and denatured states. For RNase A, however, the NMRD data show that the denatured state does not contain any long-lived water molecules ($\beta_D = 0$) and therefore only adds a frequency-independent contribution (α_D) to R_1. We can therefore use eq 2 to describe the ^{17}O NMRD data at all temperatures and interpret the parameters α and β according to

$$\alpha N_T/R_{bulk} = f_N N_{\alpha N} \rho_N + (1 - f_N) N_{\alpha D} \rho_D \tag{7}$$

$$\beta N_T/\omega_Q{}^2 = f_N N_{\beta N} S^2 \tag{8}$$

with S and τ_β pertaining to the long-lived water molecules associated with the native protein.

Analysis of ^{2}H NMRD Data. The analysis of ^{2}H NMRD data is complicated by labile hydrogens in the protein that mix with the water hydrogen pool on the relaxation time scale (ca. 100 μs). In general, the ^{2}H dispersion amplitude therefore contains contributions from both long-lived water molecules and labile hydrogens (*42*, *43*). The water contribution, β_W, is described by eq 8, where S now is the water ^{2}H order parameter which generally differs from the water ^{17}O order parameter (*20*). The labile-hydrogen contribution, β_L, can be expressed as

$$\beta_L = f_N \beta_{LN} + (1 - f_N) \beta_{LD} \tag{9}$$

Whereas the loss of all long-lived water sites on denaturation causes the ^{17}O dispersion to vanish, the labile-hydrogen contribution ensures that also the denatured protein will exhibit a ^{2}H dispersion. If all contributing labile hydrogens exchange rapidly compared to their intrinsic relaxation rates,

$$\beta_{LN} 2N_T/\omega_{QL}{}^2 = N_{LN} S_{LN}{}^2 \tag{10}$$

and similarly for β_{LD}. Here, N_{LN} is the number of rapidly exchanging labile hydrogens in the native protein with root-mean-square order parameter S_{LN} and (average) quadrupole frequency ω_{QL}. Via S_{LD}, the ^{2}H dispersion provides information about the internal flexibility of the denatured protein.

In the simplest case, where $\tau_W \gg \tau_R$, the water and labile-hydrogen contributions are additive: $\beta = \beta_W + \beta_L$. However, if τ_W is comparable to τ_R, as is the case here, the ^{2}H dispersion is bi-Lorentzian. Furthermore, since the native and denatured forms should have different tumbling times τ_R, even the labile-hydrogen contribution to the ^{2}H dispersion should be bi-Lorentzian in the transition region. This difference is expected to be much smaller than that between τ_R and τ_W and will be ignored. The parameters β_L and τ_R were determined by fitting a bi-Lorenztian function to the ^{2}H NMRD data, with β_W and τ_β obtained from the corresponding ^{17}O dispersion and an assumed value for $S^2(^2\text{H})/S^2(^{17}\text{O})$. Thus, only three parameters were adjusted. The reported parameter values were obtained by setting $S^2(^2\text{H})/S^2(^{17}\text{O}) = 0.366$, as expected for water molecules that flip around their dipole axis at a rate faster than $1/\tau_\beta$ (*20*). Librational motions then have virtually no effect on the order parameter ratio (*21*). For a rigidly bound water molecule, $S^2(^2\text{H})/S^2(^{17}\text{O}) = 1$. This limit is not appropriate for RNase A, since the water molecules that contribute to the dispersion are located in surface pockets and have relatively short residence times. Since water molecules account for only a small fraction of the ^{2}H dispersion, the derived parameters are insensitive to the assumed $S^2(^2\text{H})/S^2(^{17}\text{O})$ value. The ^{2}H NMRD profiles and fits are shown in Figure 3, with the

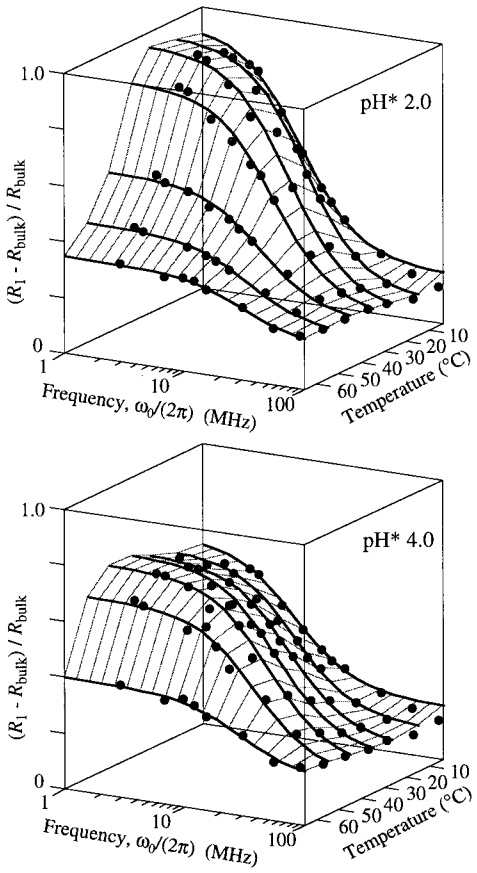

FIGURE 3: Frequency dependence of water ^{2}H longitudinal relaxation rate, R_1, normalized with the bulk water relaxation rate, from 3.76 mM solutions of RNase A in D_2O at pH* 2.0 (top) and pH* 4.0 (bottom) and at seven temperatures. The fitted curves are bi-Lorentzian dispersions, with two parameters obtained from the corresponding ^{17}O dispersion and the three adjustable parameters as given in Table 2.

resulting parameters in Table 2. As for ^{17}O, one or two high-frequency points were omitted in the fits to the 4 and 15 °C data.

RESULTS AND DISCUSSION

Loss of Long-Lived Water Molecules. It is evident from Figure 2 that the ^{17}O dispersion in the 1−100 MHz window, due to long-lived water molecules, vanishes at temperatures where the denatured state predominates. According to the CD data in Figure 1, $f_N = 0.0009$ (pH* 2) and 0.06 (pH* 4) at 65 °C. Since the correlation time τ_β reflects thermally activated processes (water exchange and protein rotation), it should decrease with increasing temperature, thereby reducing the dispersion amplitude and ultimately shifting the dispersion out of the experimental frequency window (i.e., above 100 MHz). Since the "trivial" temperature effect on the dispersion amplitude (via the viscosity dependence of the rotational correlation time) is nearly compensated for in Figure 2 by normalization with the temperature-dependent bulk water relaxation rate R_{bulk}, the variation in dispersion step must be caused mainly by a reduction of the amplitude parameter β as the protein is denatured. (The decrease of the dispersion step outside the transition region reflects the shortening of τ_β by water exchange, as demonstrated by the following analysis.)

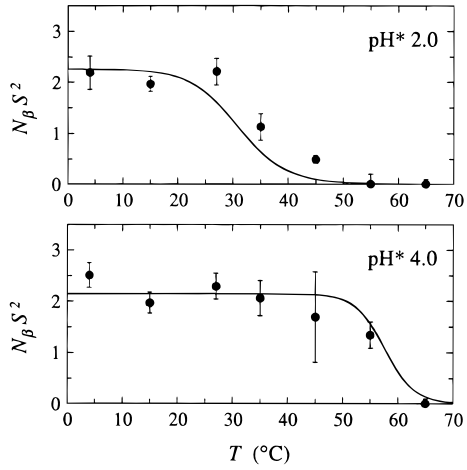

FIGURE 4: Temperature dependence of the reduced β parameter, $N_\beta S^2$, derived from the ^{17}O dispersions in Figure 2. The curves are one-parameter fits based on eqs 1 and 8.

The effect of thermal denaturation on RNase A hydration is more clearly seen by examining the temperature dependence of the dispersion parameters α and β. Figure 4 shows the reduced β parameter derived from the ^{17}O dispersions. The curves are one-parameter fits based on eqs 1 and 8, yielding $N_\beta S^2 = 2.3 \pm 0.1$ at pH* 2 and $N_\beta S^2 = 2.1 \pm 0.1$ at pH* 4. The transition temperature T_d and width ΔT were fixed at the values derived from the CD data in Figure 1. The denaturation transition is clearly manifested in the NMRD data. At pH* 4 the NMRD and CD transition temperatures coincide within experimental error, but at pH* 2, the data in Figure 4 suggest a ca. 5 °C shift of T_d.

Since RNase A does not contain any internal water molecules, the ^{17}O dispersion from the native protein must be due to long-lived water molecules partly buried in surface pockets. An examination of the 1.26 Å crystal structure 7RSA (*23*) reveals six potentially long-lived water sites (see Figure 5) with low accessibility to external solvent (≤ 7 Å^2), relatively low thermal B factor (10−20 Å^2), and at least two hydrogen bonds to the protein backbone. In phosphate-bound RNase A, two of these water molecules (the pair in the foreground of Figure 5) are displaced by the side chain of Gln 101 (*23, 44, 45*). The accumulated ^{17}O NMRD results from a variety of proteins (*19*) suggest that the long-lived water molecules responsible for the present ^{17}O dispersion are among the ones shown in Figure 5. Since perfect orientational order ($S = 1$) is unlikely for such water molecules (*46*), the $N_\beta S^2$ values obtained here show that native RNase A contains at least three long-lived ($\tau_W > 1$ ns) water molecules and that this number is essentially the same at pH* 2 and 4. The finding that $N_\beta S^2 = 0$ above the transition shows that, in the denatured protein, these water sites are either absent or have subnanosecond residence times. Furthermore, the quantitative agreement between the CD and NMRD transition temperatures at pH* 4 is consistent with a two-state model for thermal denaturation of RNase A (*27*). The somewhat higher T_d suggested by the NMRD data at pH* 2 may indicate that the initially formed denatured state contains one or two long-lived water molecules which are lost as the temperature is further increased. On the other hand, the ^{17}O NMRD data rule out intermediate states with extensive (and long-lived) internal hydration.

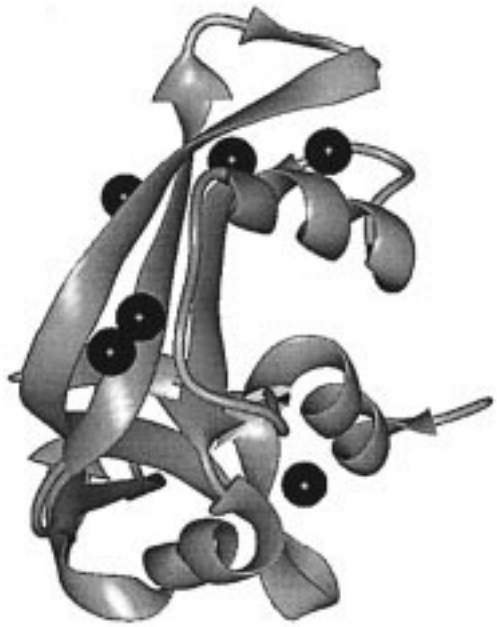

FIGURE 5: Ribbon diagram of phosphate-free RNase A based on the 1.26 Å crystal structure 7RSA (*23*). The oxygen atoms of six potentially long-lived water molecules residing in surface pockets are shown as dark spheres.

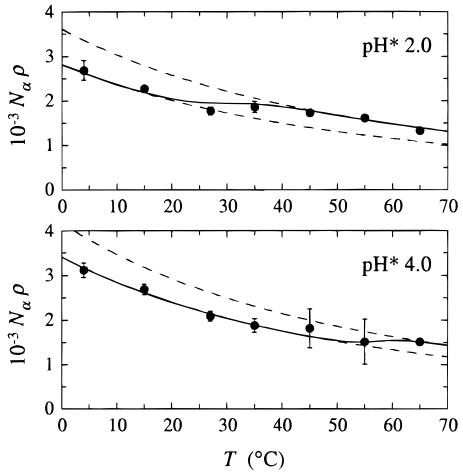

FIGURE 6: Temperature dependence of the reduced α parameter, $N_\alpha\, \rho$, derived from the ^{17}O dispersions in Figure 2. The curves are three-parameter fits based on eqs 1 and 7.

Global Solvent Exposure. Figure 6 shows the reduced α parameter derived from the ^{17}O dispersions. The curves are three-parameter fits based on eqs 1 and 7. Since the dynamic retardation factor ρ involves a ratio of correlation times (see Materials and Methods) that may have different activation energies, it is expected to vary with temperature. For the fits in Figure 6, we have set $\rho_N = \rho_D$ and fixed T_d and ΔT at the values derived from the CD data in Figure 1. The fitted parameters are the composite parameter $N_{\alpha N}\rho_N$ for the native protein at 27 °C (for comparison with previous results for other proteins at this temperature), the relative solvent exposure of the denatured protein, $N_{\alpha D}/N_{\alpha N}$, and the difference in activation energy, $\Delta E^{\#}$, for the local correlation time of water molecules at the protein surface and in bulk water.

For the quantity $N_{\alpha N}\rho_N$ at 27 °C, the fits in Figure 6 yield 1800 ± 110 at pH* 2 and 2140 ± 70 at pH* 4. With a solvent accessible area of 70.5 nm^2 for RNase A (*19*) and assuming that a water molecule occupies on average 0.15 nm^2, we estimate that ca. 470 water molecules are in contact with the protein surface. The dynamic retardation factor ρ_N at 27 °C thus becomes 3.8 ± 0.2 at pH* 2 and 4.6 ± 0.2 at pH* 4. These values are in the range 4−6 found for all proteins (*19*) that do not contain clusters of several buried water molecules (where intersite exhange can contribute significantly to α). A previous NMRD study of RNase A at pH* 2.5 and 27 °C (*19*) gave higher values for both α and β, corresponding to $N_\beta S^2 = 3.5 \pm 0.4$ and $\rho_N = 7.6 \pm 0.4$. At present, it is not clear whether this difference is real or is an artifact caused by the lower purity of the earlier protein sample.

The differential activation energy $\Delta E^{\#}$ obtained from the fits in Figure 6 is 12 ± 2 kJ mol^{-1} at both pH* values. This is in the expected range. Water ^{17}O relaxation studies of aqueous solutions of short-chain alcohols yield activation energies of 8−20 kJ mol^{-1} for the dynamic retardation factor (*47*). Similarly, $\Delta E^{\#}$ values of 9 and 17 kJ mol^{-1} were found for water associated with the oxyethylene segments of poly(ethylene oxide) (*48*) and $C_{12}E_8$ micelles (*49*), respectively.

The relative solvent exposure, $N_{\alpha D}/N_{\alpha N}$, of thermally denatured RNase A obtained from the fits in Figure 6 is 1.3 ± 0.2 at pH* 2 and 1.2 ± 0.1 at pH* 4. If the assumption $\rho_N = \rho_D$ (i.e., the same average dynamic retardation of water in contact with the native and denatured protein surfaces) is accepted, these values can be interpreted as the ratio of the solvent-accessible areas for the two states. For complete unfolding (to an extended β conformation) of native RNase A, the solvent-accessible area increases by ca. 100 nm^2 (*6, 12, 50*−*52*). It has been argued that the four disulfide bonds of RNase A should reduce this value by ca. 34 nm^2 (*52*). We would thus expect $N_{\alpha D}/N_{\alpha N} = 1 + (100-34)/70.5 = 1.9$ for maximum unfolding of disulfide-intact RNase A. The smaller values obtained here suggest that thermally denatured RNase A is significantly more compact, in agreement with scattering data (*24, 25*). We cannot, however, exclude the possibility that a larger increase of N_α on denaturation is partly compensated by a decrease of ρ.

Side-Chain Disorder. Like the ^{17}O dispersions in Figure 2, the ^{2}H dispersions in Figure 3 clearly reflect the thermal denaturation transition. There are two qualitative differences, however, between the ^{17}O and ^{2}H dispersions. First, a sizable ^{2}H dispersion remains even at the highest temperature. Second, the ^{2}H dispersion amplitude increases markedly with temperature outside the transition region. These are the hallmarks of a dominant labile-hydrogen contribution to the ^{2}H dispersion.

Figure 7 shows the labile-hydrogen contribution, β_L, to the ^{2}H dispersion, determined from the bi-Lorentzian fits in Figure 3 with the water contribution taken from the ^{17}O results (see Materials and Methods). As in Figure 4, the denaturation transition is clearly evident. The curves are three-parameter fits based on eqs 1 and 9 with T_d and ΔT taken from the CD data. The adjusted parameters are β_{LN} (27 °C), β_{LD}/β_{LN}, and an apparent activation energy, taken to be the same for β_{LN} and β_{LD}, that essentially determines the rate of increase of the number of rapidly exchanging labile hydrogens as their exchange rate constants increase with temperature.

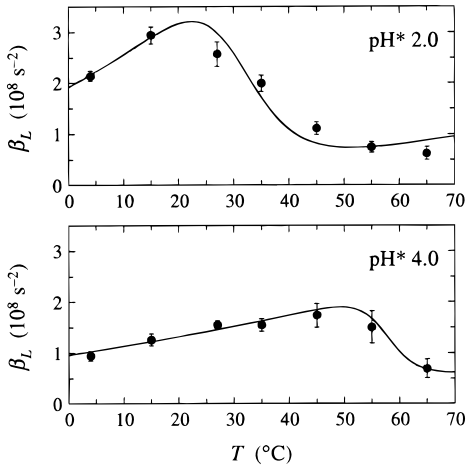

FIGURE 7: Temperature dependence of the labile-hydrogen contribution, β_L, to the ^{2}H dispersion step in Figure 3. The curves are three-parameter fits based on eqs 1 and 9.

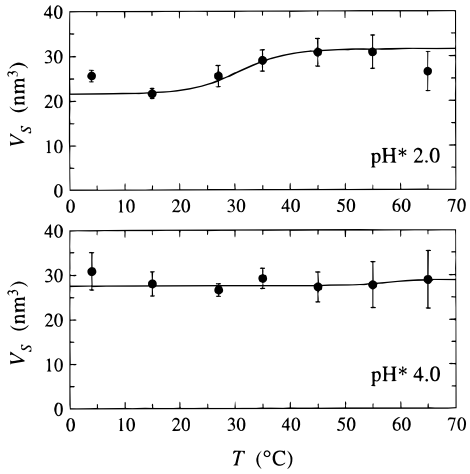

FIGURE 8: Temperature dependence of the hydrodynamic volume, V_S, derived from the rotational correlation time of the labile-hydrogen contribution to the ^{2}H dispersions in Figure 3. The curves are two-parameter fits based on eqs 1 and 9 (with β replaced by τ_R).

Bovine pancreatic RNase A contains 11 carboxyl groups and 31 hydroxyl groups. If a minor contribution from the four histidines is ignored, the labile hydrogens responsible for the β_L dispersion must reside in these COOH and OH groups. The rate constant, k_1, for acid-catalyzed hydrogen exchange from OH groups in proteins should be on the order of 1×10^7 M^{-1} s^{-1} at 27 °C (*53*, *54*). At pH* 2, these hydroxyl hydrogens should therefore be in the fast-exchange limit, contributing fully to β_L. Allowing for a few OH groups with smaller rate constants (two tyrosines are buried), we take $N_{LN} = 35$ as an estimate for the native protein at pH* 2 and 27 °C. With $N_T = 14\,140$, $\omega_{QL} = 7.7 \times 10^5$ rad s^{-1} (*55*), and the values β_{LN} (27 °C, pH* 2) = $(4.0 \pm 0.2) \times 10^8$ s^{-2} and β_{LN} (27 °C, pH* 4) = $(1.5 \pm 0.1) \times 10^8$ s^{-2} derived from the fits, eq 10 yields $N_{LN}S_{LN}^2 = 19 \pm 1$ at pH* 2 and 7.0 ± 0.2 at pH* 4. The former value corresponds to $S_{LN}^2 = 0.55 \pm 0.03$ as an average over 35 OH and COOH groups. The nearly 3-fold reduction of β_{LN} at pH* 4 is due to deprotonation of six of the COOH groups (*56*) and to 100-fold slower hydrogen exchange from the OH groups. The effective number of rapidly exchanging hydrogens, $N_{LN} = 7.0/0.55 = 13$, indicates that about one-third of the accessible OH groups contribute to β_{LN} at pH* 4 and 27 °C. The effective hydrogen exchange rate, $k_1\,10^{-pH*}$, should then be roughly half of the intrinsic relaxation rate, $\omega_{QL}^2 S_{LN}^2 \tau_R = (7.7 \times 10^5)^2 \times 0.41 \times (6.6 \times 10^{-9}) = 1.6 \times 10^3$ s^{-1}. This requires that $k_1 \approx 0.8 \times 10^7$ M^{-1} s^{-1}, which is of the expected order of magnitude (*53*, *54*).

The pronounced reduction of β_L on thermal denaturation (see Figure 7) is direct evidence for enhanced internal flexibility in the denatured protein. At pH* 2, the ratio $\beta_{LD}/\beta_{LN} = 0.09 \pm 0.02$ obtained from the fit indicates that the mean-square order parameter for O−H bonds in ca. 35 Asp, Glu, Ser, Thr, and Tyr residues drops from 0.55 to 0.05 on thermal denaturation. This large effect can probably be attributed to local side-chain disorder, although more extensive structural fluctuations may also contribute to the orientational averaging. At pH* 4, the effect is somewhat smaller, $\beta_{LD}/\beta_{LN} = 0.24 \pm 0.09$. If S_{LN}^2 is the same as at pH* 2, we obtain $S_{LD}^2 = 0.13$ for the O−H bonds in ca. 13 residues that contribute to β_L at pH* 4. Although nearly all COOH and OH groups are solvent exposed in the native protein, denaturation should lead to somewhat faster hydrogen exchange (larger k_1), making $N_{LD} > N_{LN}$ at a given temperature. Some carboxyl pK_a shifts are also expected. Both of these effects should be negligible at pH* 2, where the OH hydrogens are already in the fast-exchange limit in the native protein and where nearly all COOH groups are protonated. At pH* 4, however, it is likely that S_{LD}^2 is somewhat overestimated by taking $N_{LD} = N_{LN}$.

Hydrodynamic Volume. The rotational correlation time of a protein as small as RNase A is much shorter than the residence times of even the fastest-exchanging labile hydrogens (at pH <11). The correlation time associated with the labile-hydrogen contribution to the ^{2}H dispersion can therefore be identified with the rotational correlation time τ_R of the protein (cf. eq 5). The rotational motion of the denatured protein can thus be monitored by the ^{2}H dispersion, even in the absence of long-lived water molecules.

The rotational correlation times derived from the ^{2}H dispersions in Figure 3 are presented in Table 2. The temperature dependence of τ_R is dominated by the 4-fold variation of the solvent (D_2O) viscosity in the range 4−65 °C. To isolate the nontrivial temperature dependence, we focus on the apparent hydrodynamic (Stokes) volume,

$$V_S = k_B T \tau_R / \eta \qquad (11)$$

For a smooth rigid sphere undergoing free rotational diffusion, V_S is simply the volume of the sphere. Figure 8 shows the temperature dependence of V_S. The fitted curves, with T_d and ΔT fixed at the values derived from the CD data, yield the hydrodynamic volumes, V_{SN} and V_{SD}, of the native and denatured states. (The 4 and 65 °C points were not included in the fit to the pH* 2 data.) While, at pH* 2, the denaturation transition is clearly manifested as an increase in V_S, the variation of V_S at pH* 4 is not significant.

For the native protein, we obatin $V_{SN} = 21.6 \pm 1.1$ nm^3 at pH* 2 and 27.6 ± 1.0 nm^3 at pH* 4. The molecular protein volume, V_P, is 16.2 nm^3 according to the crystal structure (*23*) or 16.0 nm^3 according to the limiting partial specific volume of RNase A in aqueous solution at 25 °C (*57*). The common finding that $V_{SN} > V_P$ is often rationalized by invoking one or two layers of "bound" water. In view of the subnanosecond residence times of virtually all

water molecules at protein surfaces, this argument is questionable. Nonsphericity (the axial ratio of RNase A is ca. 1.5) and surface roughness (*58*) can probably account for most of the discrepancy between V_{SN} and V_P for dilute protein solutions. For more concentrated solutions, protein−protein interactions may also retard protein tumbling, thereby increasing the apparent hydrodynamic volume. The substantial pH dependence of V_{SN} suggests that this is the case for RNase A at our protein concentration of 3.76 mM. With the higher net charge (+18) at pH* 2, the Coulomb repulsion (in our salt-free solution) can presumably overcome the short-range attractive forces that more effectively slow protein rotation at pH* 4 (net charge +12). The nearly 30% difference in V_{SN} between pH* 2 and 4 could also reflect a pH dependence of the native protein structure. This is unlikely, however, since $N_\beta S^2$ is the same at pH* 2 and 4 (see Figure 4).

Since protein−protein interactions appear to be significant under the present conditions (at least at pH* 4), the variation of V_S on denaturation must be interpreted with caution. At pH* 4, the expected ca. 50% increase of V_S on thermal denaturation (*25, 59*) may thus be masked by a compensating difference in protein−protein interactions for the native and denatured states. At pH* 2, V_{SN} is close to the expected value and probably less affected by protein−protein interactions. The fit in Figure 8 yields $V_{SD} = 31.5 \pm 2.0$ nm^3, i.e., the relative expansion is $V_{SD}/V_{SN} = 1.5 \pm 0.1$. This is significantly less than the value, $V_{SD}/V_{SN} = 2.0$, derived from a time-domain dielectric relaxation study of the thermal denaturation of RNase A at pH 2.6 (*60*). The (collective) translational diffusion coefficient measured by DLS for thermal denaturation of RNase A at pH 2 yields for V_{SD}/V_{SN} 1.22 (10 mM KCl) and 1.64 (150 mM KCl) (*61*). A more recent DLS study (*25*), however, demonstrated large virial effects at pH 2.5. At pH 4 (10 mM sodium acetate, 20 °C), the DLS diffusion coefficient extrapolated to zero protein concentration (to eliminate virial effects) yields $V_{SU}/V_{SN} = 2.6 \pm 0.2$, where V_{SU} refers to disulfide-intact RNase A in 6 M GdmCl (*25*). In light of these results, the 50% expansion obtained here indicates that the thermally denatured state is rather compact even at pH* 2.

Residence Time of Long-Lived Water Molecules. At all investigated temperatures and pH* values, the correlation time τ_β derived from the ^{17}O dispersions is significantly shorter than the rotational correlation time τ_R deduced from the labile-hydrogen contribution to the ^{2}H dispersion (see Tables 1 and 2). Although such differences have been observed for several other proteins (*19*), the effect is much larger for RNase A. The finding that $\tau_\beta < \tau_R$ indicates that the water residence time τ_W is not much longer than τ_R, cf. eq 5. This is indeed expected for RNase A, where the water molecules responsible for the ^{17}O dispersion are located in surface pockets rather than in internal cavities (see Figure 5). The water residence times computed from eq 5 with τ_β and τ_R data from Tables 1 and 2 are shown in the Arrhenius plot of Figure 9. Of course, τ_W can only be determined at temperatures where the population of the native state is sufficient to produce a significant ^{17}O dispersion. No systematic difference in τ_W is seen between pH* 2 and 4, consistent with the indication from the ^{17}O β value that the native protein structure is invariant in this pH range. Consequently, all 10 τ_W values in Figure 9 were included in the fit, yielding $\tau_W = 7.6 \pm 1.3$ ns at 27 °C and an activation enthalpy of 43 ± 10 kJ mol^{-1}. This is comparable to the activation enthalpy of 52 ± 3 kJ mol^{-1} recently determined for exchange of the ordered water molecules in the minor groove of several DNA dodecamer duplexes (*21*), but, as expected, much smaller than the 90 ± 5 kJ mol^{-1} obtained for the exchange of a deeply buried water molecule in BPTI (*62*).

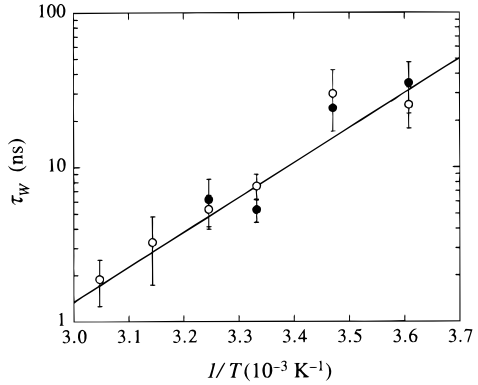

FIGURE 9: Temperature dependence of the water residence time, τ_W, derived from the ^{17}O and ^{2}H correlation times according to eq 5. The line resulted from an Arrhenius fit including data at pH* 2.0 (●) and pH* 4.0 (○).

CONCLUSIONS

The present work demonstrates that the ^{17}O/^{2}H NMRD method, previously used to study the hydration and dynamics of native biomolecules (*19, 20*), can also provide valuable information about denatured proteins in solution. The structure and dynamics of the protein is probed by specific long-lived water molecules as well as by the global hydration and labile side-chain hydrogens.

Since long-lived water molecules are only found in internal cavities and in deep surface pockets, a completely unfolded, random-coillike protein is not expected to retain any long-lived water sites and, therefore, should not exhibit any water ^{17}O relaxation dispersion below 100 MHz. In a partially folded protein, however, the combination of extensive water penetration and residual protein structure might lead to the formation of new long-lived water sites. Such water sites will be sufficiently long-lived to produce an ^{17}O dispersion only if the local structure is maintained on a nanosecond time scale.

The present study shows that native RNase A contains at least three water molecules with a mean residence time of 8 ns at 27 °C and an activation enthalpy of ca. 40 kJ mol^{-1}. The current understanding of the determinants of water exchange rates (*19*) strongly suggests that these moderately long-lived water molecules can be identified with some or all of the six ordered water molecules that are partly buried in surface pockets in the crystal structure of RNase A (see Figure 5). The loss of the ^{17}O dispersion at higher temperatures (see Figure 4) demonstrates that, in the thermally denatured protein, these surface pockets are either not present or undergoing large structural fluctuations on a subnanosecond time scale. Furthermore, the finding that the dispersion step (β parameter) vanishes monotonically and essentially in parallel with the CD denaturation curves is consistent with a two-state model where the loss of long-lived water sites

coincides with the disruption of the native secondary and tertiary structure. Although the slight difference between the NMRD and CD denaturation temperatures at pH* 2 may indicate a temperature-dependent hydration of the denatured state, we find no evidence for partly folded equilibrium intermediates with a large amount of non-native long-lived hydration.

The picture of thermally denatured RNase A emerging from the present NMRD study is that of a highly flexible but relatively compact structure. The mean-square orientational order parameter S^2 of O−H bonds in side chains at the surface of RNase A is strongly reduced on thermal denaturation. In the denatured state, these side chains must sample a wide distribution of conformational states on a subnanosecond time scale. The global increase of solvent exposure on thermal denaturation is roughly one-third of that expected for the maximally unfolded disulfide-intact protein. Thermal denaturation increases the hydrodynamic volume by a modest 50% at pH* 2, much less than for disulfide-intact RNase A denatured in 6 M GdmCl (260%). While we cannot claim quantitative accuracy regarding solvent exposure (the dynamic retardation factor ρ may differ between native and denatured states) and hydrodynamic volume (protein−protein interactions may affect τ_R differently in native and denatured states), the results on α and τ_R reinforce each other and are consistent with a host of other observations that indicate substantial residual structure in the heat-denatured state of RNase A.

ACKNOWLEDGMENT

We are grateful to Eva Thulin for protein purification.

REFERENCES

1. Tanford, C. (1968) *Adv. Protein Chem. 23*, 121−282.
2. Dill, K. A., and Shortle, D. (1991) *Annu. Rev. Biochem. 60*, 795−825.
3. Dobson, C. M. (1992) *Curr. Opin. Struct. Biol. 2*, 6−12.
4. Shortle, D. (1993) *Curr. Opin. Struct. Biol. 3*, 66−74.
5. Shortle, D. (1996) *FASEB J. 10*, 27−34.
6. Robertson, A. D., and Murphy, K. P. (1997) *Chem. Rev. 97*, 1251−1267.
7. Matthews, C. R. (1993) *Annu. Rev. Biochem. 62*, 653−683.
8. Miranker, A., and Dobson, C. M. (1996) *Curr. Opin. Struct. Biol. 6*, 31−42.
9. Neira, J. L., and Rico, M. (1997) *Folding Des. 2*, R1−R11.
10. Kauzmann, W. (1959) *Adv. Protein Chem. 14*, 1−63.
11. Tanford, C. (1997) *Protein Sci. 6*, 1358−1366.
12. Makhatadze, G. I., and Privalov, P. L. (1994) *Biophys. Chem. 51*, 291−309.
13. Tamura, Y., and Gekko, K. (1995) *Biochemistry 34*, 1878−1884.
14. Daggett, V., and Levitt, M. (1992) *Proc. Natl. Acad. Sci. U.S.A. 89*, 5142−5146.
15. Mark, A. E., and van Gunsteren, W. F. (1992) *Biochemistry 31*, 7745−7748.
16. Caflisch, A., and Karplus, M. (1994) *Proc. Natl. Acad. Sci. U.S.A. 91*, 1746−1750.
17. Williams, M. A., Thornton, J. M., and Goodfellow, J. M. (1997) *Protein Eng. 10*, 895−903.
18. Hünenberger, P. H., Mark, A. E., and van Gunsteren, W. F. (1995) *Proteins 21*, 196−213.
19. Denisov, V. P., and Halle, B. (1996) *Faraday Discuss. 103*, 227−244.
20. Halle, B., Denisov, V. P., and Venu, K. (1998) in *Modern Techniques in Protein NMR* (Berliner, L. J., and Krishna, N. R., Eds.), Vol. 16B, Plenum, New York, in press.
21. Jóhannesson, H., and Halle, B. (1998) *J. Am. Chem. Soc*. (In press).
22. Santoro, J., Gonzalez, C., Bruix, M., Neira, J. L., Nieto, J. L., Herranz, J., and Rico, M. (1993) *J. Mol. Biol. 229*, 722−734.
23. Wlodawer, A., Svensson, L. A., Sjölin, L., and Gilliland, G. L. (1988) *Biochemistry 27*, 2705−2717.
24. Sosnick, T. R., and Trewhella, J. (1992) *Biochemistry 31*, 8329−8335.
25. Nöppert, A., Gast, K., Müller-Frohne, M., Zirwer, D., and Damaschun, G. (1996) *FEBS Lett. 380*, 179−182.
26. Hermans, J., and Scheraga, H. A. (1961) *J. Am. Chem. Soc. 83*, 3283−3292.
27. Ginsburg, A., and Carroll, W. R. (1965) *Biochemistry 4*, 2159−2174.
28. Tsong, T. Y., Hearn, R. P., Wrathall, D. P., and Sturtevant, J. M. (1970) *Biochemistry 9*, 2666−2677.
29. Aune, K. C., Salahuddin, A., Zarlengo, M. H., and Tanford, C. (1967) *J. Biol. Chem. 242*, 4486-4489.
30. Matthews, C. R., and Froebe, C. L. (1981) *Macromolecules 14*, 452−453.
31. Labhardt, A. M. (1982) *J. Mol. Biol. 157*, 331−355.
32. Seshadri, S., Oberg, K. A., and Fink, A. L. (1994) *Biochemistry 33*, 1351−1355.
33. Takeda, N., Kato, M., and Taniguchi, Y. (1995) *Biochemistry 34*, 5980−5987.
34. Fabian, H., and Mantsch, H. H. (1995) *Biochemistry 34*, 13651−13655.
35. Robertson, A. D., and Baldwin, R. L. (1991) *Biochemistry 30*, 9907−9914.
36. Privalov, P. L., Tiktopulo, E. I., Venyaminov, S. Yu., Griko, Yu. V., Makhatadze, G. I., and Khechinashvili, N. N. (1989) *J. Mol. Biol. 205*, 737−750.
37. Privalov, P. L., and Makhatadze, G. I. (1990) *J. Mol. Biol. 213*, 385−391.
38. Edelhoch, H. (1967) *Biochemistry 6*, 1948−1954.
39. Makhatadze, G. I., Clore, G. M., and Gronenborn, A. M. (1995) *Nat. Struct. Biol. 2*, 852−855.
40. Denisov, V. P., and Halle, B. (1995) *J. Mol. Biol. 245*, 682−697.
41. Abragam, A. (1961) *The Principles of Nuclear Magnetism*, Clarendon, Oxford.
42. Piculell, L., and Halle, B. (1986) *J. Chem. Soc., Faraday Trans. 1 82*, 401−414.
43. Denisov, V. P., and Halle, B. (1995) *J. Mol. Biol. 245*, 698−709.
44. Zegers, I., Maes, D., Dao-Thi, M.-H., Poortmans, F., Palmer, R., and Wyns, L. (1994) *Protein Sci. 3*, 2322−2339.
45. Kishan, K. V. R., Chandra, N. R., Sudarsanakumar, C., Suguna, K., and Vijayan, M. (1995) *Acta Crystallogr., Sect. D 51*, 703−710.
46. Denisov, V. P., Venu, K., Peters, J., Hörlein, H. D., and Halle, B. (1997) *J. Phys. Chem. B 101*, 9380−9389.
47. Ishihara, Y., Okouchi, S., and Uedaira, H. (1997) *J. Chem. Soc., Faraday Trans. 1 93*, 3337−3342.
48. Breen, J., Huis, D., de Bleijser, J., and Leyte, J. C. (1988*) J. Chem. Soc., Faraday Trans. 1 84*, 293−307.
49. Carlström, G., and Halle, B. (1989) *J. Chem. Soc., Faraday Trans. 1 85*, 1049−1063.
50. Livingstone, J. R., Spolar, R. S., and Record, M. T. (1991) *Biochemistry 30*, 4237−4244.
51. Spolar, R. S., Livingstone, J. R., and Record, M. T. (1992) *Biochemistry 31*, 3947−3955.
52. Myers, J. K., Pace, C. N., and Scholtz, J. M. (1995) *Protein Sci. 4*, 2138−2148.
53. Liepinsh, E., and Otting, G. (1996) *Magn. Reson. Med. 35*, 30−42.
54. Liepinsh, E., Otting, G., and Wüthrich, K. (1992) *J. Biomol. NMR 2*, 447−465.
55. Hunt, M. J., and Mackay, A. L. (1974) *J. Magn. Reson. 15*, 402−414.

56. Baker, W. R., and Kintanar, A. (1996) *Arch. Biochem. Biophys. 327*, 189−199.
57. Chalikian, T. V., Totrov, M., Abagyan, R., and Breslauer, K. J. (1996) *J. Mol. Biol. 260*, 588−603.
58. Garcia de la Torre, J., and Bloomfield, V. A. (1981) *Q. Rev. Biophys. 14*, 81−139.
59. Gast, K., Zirwer, D., Damaschun, H., Hahn, U., Müller-Frohne, M., Wirth, M., and Damaschun, G. (1997) *FEBS Lett. 403*, 245−248.
60. Feldman, Yu. D., and Fedotov, V. D. (1988) *Chem. Phys. Lett. 143*, 309−312.
61. Nicoli, D. F., and Benedek, G. B. (1976) *Biopolymers 15*, 2421−2437.
62. Denisov, V. P., Peters, J., Hörlein, H. D., and Halle, B. (1996) *Nat. Struct. Biol. 3*, 505−509.

BI980442B